Pergamon

Int. J. Heat Mass Transfer. Vol. 37, No. 14, pp. 2025–2033, 1994

0017–9310/94 $7.00 + 0.00

0017–9310(94)E0049–Z

Heat transfer from pulsating flow in a channel filled with porous media

SEO YOUNG KIM,† BYUNG HA KANG‡ and JAE MIN HYUN†§

†Department of Mechanical Engineering, Korea Advanced Institute of Science and Technology, Yusung-ku, Taejon, 305-701, South Korea

‡Thermal/Fluids Engineering Laboratory, Korea Institute of Science and Technology, Cheongryang, P.O. Box 151, Seoul, South Korea

(*Received* 21 *October* 1993 *and in final form* 10 *February* 1994)

Abstract—A numerical study is made of heat transfer characteristics from forced pulsating flow in a channel filled with fluid-saturated porous media. The channel walls are assumed to be at uniform temperature. The Brinkman–Forchheimer-extended Darcy model is employed. The time-dependent, two-dimensional governing equations are solved by using finite-volume techniques. Numerical solutions are obtained for quasi-steady periodic states. Flow and temperature fields are examined over ranges of the principal parameters, i.e. the amplitude of flow pulsation A, the pulsation frequency parameter M $[\equiv H(\omega/2\nu)^{1/2}]$, the Darcy number Da $(\equiv K/H^2)$, the thermal conductivity ratio R_k $(\equiv k_{eff}/k)$, and the heat capacity ratio R_c $\{\equiv(\rho C_p)_{eff}/[\varepsilon(\rho C_p)]\}$. The impact of pulsation is discernible in the cycle-averaged temperature distribution. In comparison with the case of non-pulsating flow, the presence of flow pulsation brings forth a reduction in heat transfer in the entrance region and an enhancement of heat transfer at moderate downstream regions. Farther downstream, the influence of pulsation is meager. The magnitudes of changes in heat transfer depend upon A, M, Da, R_k, and R_c. The effect of pulsation on heat transfer between the channel wall and the fluid is more pronounced for small M and large A. Explicit influences of Da, R_k, and R_c on the flow and heat transport characteristics are also scrutinized.

1. INTRODUCTION

CONSIDERABLE attention has been given lately to forced convective flow and heat transfer properties of pulsating flow in a confined passageway. The subject matter is of interest from the viewpoint of basic research of unsteady forced convection. Also, the study is of immediate relevance to a multitude of technological applications, e.g. from reciprocating engine to human circulatory system, to cite a few. The salient characteristics of a confined pulsating flow were investigated in earlier treatises by Uchida [1], and studies of the associated heat transfer properties were carried out by Lighthill [2], Siegel and Perlmutter [3] and Kurzweg [4], among others. Recently, with the advent of high-performance Stirling engines, there has been a growing need to achieve augmented heat transfer from pulsating fluid flow. One such effort has been directed to exploring the use of a porous matrix inside the fluid passageway. In particular, industrial applications of using a pulsating flow in a highly porous channel were elaborated [5].

The features of heat transfer in saturated porous media, with a non-pulsating through-flow, have constituted a classical topic [6–8]. These investigations have been motivated by various applications in geophysics and energy engineering disciplines. These prior undertakings disclosed prominent characteristics of non-pulsating flow and heat transfer in porous media. Furthermore, the non-Darcian effects on thermal convection inside porous media have been addressed. In particular, Kaviany [9] dealt with heat transfer from a non-pulsating laminar through-flow confined between two parallel plates maintained at constant temperature. A similar problem was also tackled by Poulikakos and Renken [10], in which the effects of flow inertia, variable porosity and the Brinkman friction were included.

As observed by Simon and Seume [5], however, fundamental studies of pulsating-flow heat transfer inside porous media in a channel are scarce and incomplete. The recent work by Khodadadi [11] treated analytically an oscillatory flow inside a porous medium, under the assumption of a fully-developed region of a channel. However, a thorough literature survey reveals that no published reports have dealt with the issue of associated heat transports. The present account is concerned with heat transfer in more realistic situations, in which both of the afore-stated dynamic effects, i.e. the flow pulsation and the porous media, are taken into consideration. Specifically,

§Author to whom correspondence should be addressed.

NOMENCLATURE

A	non-dimensional flow pulsation amplitude
B	axial pressure gradient, $-(\partial P/\partial X)$
C	inertia coefficient
C_f	skin friction coefficient, $\sigma_w/(\frac{1}{2}\rho U_0^2)$
C_p	specific heat of fluid
Da	Darcy number, K/H^2
H	half-width of flow channel
k	thermal conductivity
K	permeability of porous medium
L_1	length of unheated section
L_2	length of heated section
M	frequency parameter, $H(\omega/2\nu)^{1/2}$
Nu	Nusselt number, $hH/k = (R_k/\theta_w)(\mathrm{d}\theta/\mathrm{d}Y)\|_{Y=1}$
Nu_b	Nusselt number based on bulk temperature, $4(\mathrm{d}\theta/\mathrm{d}Y\|_{Y=1})/(1-\theta_b)$
P	pressure
Pr	Prandtl number, ν/α
Pr'	modified Prandtl number, εPr
R_c	heat capacity ratio, $(\rho C_p)_{eff}/[\varepsilon(\rho C_p)]$
R_k	thermal conductivity ratio, k_{eff}/k
Re	Reynolds number, $U_0 H/\nu$
t	dimensionless time
T	dimensional temperature
u, v	dimensional velocity components
U, V	dimensionless velocity components
u'	fluctuating part of velocity
U_{t-s}	normalized time-dependent velocity, $U'/(B_1/B_m)$
x, y	dimensional axial and transverse coordinates
X, Y	dimensionless axial and transverse coordinates
X^*	inverse of the Graetz number, $X/(Re\,Pr)$.

Greek symbols

α	thermal diffusivity, $k/\rho C_p$
ε	porosity of porous medium
θ	dimensionless temperature
θ_b	bulk temperature, $\int_0^1 U\theta\,\mathrm{d}Y/\int_0^1 U\,\mathrm{d}Y$
ν	kinematic viscosity
ρ	density
σ_w	shear stress
τ	dimensional time.

Subscripts

1	primary oscillating component
eff	effective value of porous medium
m	time mean value
max	maximum
min	minimum
o	reference
s	non-pulsating component
t	overall time-dependent values.

numerical solutions are sought to the basic governing equations to depict the features of unsteady convective heat transport in a porous material-filled channel.

Efforts are focused on identifying the influence of respective non-dimensional parameters on local heat transfer properties. The flow at the channel inlet is assumed to contain a well-defined single-frequency pulsation component. By numerically solving the governing equations, the details of both flow and thermal fields are acquired. The objective is to describe the axially-varying heat transfer between the channel wall and the fluid. The numerical results are expected to provide an improved understanding of the underlying physical phenomena. This study also aims to construct a baseline framework for predicting heat transfer and flow features of more complex configurations. This aspect is significant in view of the lack of documented experimental and/or numerical data on heat transport from pulsating flows in a porous medium-filled channel.

2. THE MODEL

Consider a two-dimensional channel filled with a fluid-saturated porous medium, as sketched in Fig. 1. The coordinates (x, y) and channel configuration, together with the Darcian velocity components, $\mathbf{v} = (u, v)$, are indicated therein. The channel walls, situated at $y = \pm H$, are assumed to be impermeable. As remarked by Siegel and Perlmutter [3], an unheated hydrodynamic entrance region of length L_1 exists at the inlet. This is followed by the channel wall of length L_2, at which constant temperature T_w is maintained. Due to the symmetry with respect to the centerline of the channel, the calculation domain was limited to a half-width of flow channel in this study.

At the inlet, the unidirectional velocity U_∞, of constant temperature T_o, contains a sinusoidal pulsation of amplitude A and frequency ω:

$$U_\infty = U_o(1 + A\cos\omega\tau), \tag{1}$$

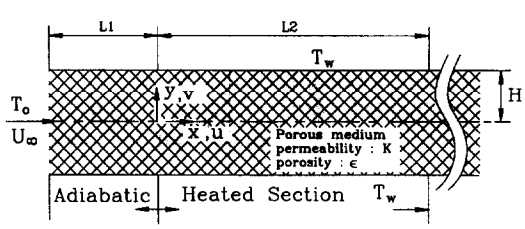

FIG. 1. Schema of flow configuration.

where τ denotes time. In conformity with the majority of preceding studies, the porous medium is taken to be homogeneous, isotropic and in local equilibrium with the fluid. The thermophysical properties of the fluid and the effective properties of the porous medium are assumed to be constant [6, 8].

With the above assumptions, the time-dependent governing equations, in properly non-dimensionalized form, can be written as, using standard notation [6, 8, 12]:

$$\nabla \cdot \mathbf{V} = 0, \tag{2}$$

$$\frac{\partial \mathbf{V}}{\partial t} + \mathbf{V} \cdot \nabla \mathbf{V} = -\nabla P + \frac{1}{Re} \nabla^2 \mathbf{V} - \left[\frac{\varepsilon}{Da \cdot Re} + \frac{\varepsilon^2 \cdot C}{\sqrt{Da}} |\mathbf{V}| \right] \mathbf{V}, \tag{3}$$

$$R_c \frac{\partial \theta}{\partial t} + \mathbf{V} \cdot \nabla \theta = \frac{R_k}{Re \cdot Pr'} \nabla^2 \theta, \tag{4}$$

in which $|\mathbf{V}| = \sqrt{U^2 + V^2}$, ε denotes the porosity, C the inertia coefficient of the porous medium and Pr' the modified Prandtl number, i.e. εPr. The momentum equation (3) represents the Brinkman–Forchheimer-extended Darcy model [6], which includes both viscous and inertia effects. It is noted that the last term in equation (3) indicates an improved model to account for the inertia effect in the momentum equation. The formulation of Khodadadi [11] does not include this term. Equation (4) is the energy equation, which is widely utilized to tackle time-dependent convective processes in porous media [12].

In the above, the non-dimensional quantities are defined as:

$$X \equiv \frac{x}{H}, \quad Y \equiv \frac{y}{H}, \quad \mathbf{V} \equiv \frac{\mathbf{v}}{\varepsilon U_o}, \quad t \equiv \frac{\tau}{H/U_o}, \quad P \equiv \frac{p - p_o}{\rho U_o^2}, \quad \theta \equiv \frac{T - T_o}{T_w - T_o}. \tag{5}$$

The dimensionless parameters in equations (2)–(4) are defined as:

Reynolds number: $Re \equiv \dfrac{U_o H}{\nu}$

Darcy number: $Da \equiv \dfrac{K}{H^2}$

Prandtl number: $Pr \equiv \dfrac{\nu}{\alpha}$

Thermal conductivity ratio: $R_k \equiv \dfrac{k_{eff}}{k}$

Heat capacity ratio: $R_c \equiv \dfrac{(\rho C_p)_{eff}}{\varepsilon (\rho C_p)}$

where ν is the kinematic viscosity, α the thermal diffusivity, and k the thermal conductivity of the fluid, while k_{eff} is the effective thermal conductivity and K the permeability of the porous medium. In equation (3), the value of the inertia coefficient C in Forchheimer's extension is taken to be equal to 0.057 [11, 13]. This value is admittedly too low for conventional sphere-shaped porous material for which the Ergun relation [14] is applicable. However, for Foametal, which is gaining popularity in advanced heat-exchanger application, C takes a much smaller value. The present account is addressed to these applications. The porosity ε is set to 0.6. While the precise value of ν_{eff} in Brinkman's extension remains somewhat unclear, ν_{eff} is taken to be the same as ν, as a first approximation as ascertained by Lundgren [15].

The associated boundary conditions are formulated as follows. At the channel inlet (at $X = -L_1$, for $0 < Y < 1$):

$$U(-L_1, Y, t) = 1 + A \sin\left(\frac{2M^2}{Re} t\right), \tag{6a}$$

$$V(-L_1, Y, t) = 0, \tag{6b}$$

$$\theta(-L_1, Y, t) = 0. \tag{6c}$$

In equation (6a), the non-dimensional pulsation frequency parameter, $M = H(\omega/2\nu)^{1/2}$, appears in the inlet flow conditions. At the channel walls ($Y = 1$, for $-L_1 < X < 0$):

$$U(X, 1, t) = 0, \tag{7a}$$

$$V(X, 1, t) = 0, \tag{7b}$$

$$\frac{\partial \theta}{\partial Y}(X, 1, t) = 0, \tag{7c}$$

and at the isothermal wall ($Y = 1$, for $0 < X < L_2$):

$$U(X, 1, t) = 0, \tag{8a}$$

$$V(X, 1, t) = 0, \tag{8b}$$

$$\theta(X, 1, t) = 1. \tag{8c}$$

Owing to the symmetry requirement at the channel centerline (at $Y = 0$, for $-L_1 < X < L_2$), it follows that:

$$\frac{\partial U}{\partial Y}(X, 0, t) = 0, \tag{9a}$$

$$V(X, 0, t) = 0, \tag{9b}$$

$$\frac{\partial \theta}{\partial Y}(X, 0, t) = 0. \tag{9c}$$

At the channel exit, the flow is assumed to have attained a fully developed state. This is a customary procedure (see Denison *et al.* [16]), invoked under the assumption that the channel is sufficiently long, i.e. $L_2 \gg 1$. Accordingly, at $X = L_2$, for $0 < Y < 1$:

$$\frac{\partial U}{\partial X}(L_2, Y, t) = 0, \tag{10a}$$

$$\frac{\partial V}{\partial X}(L_2, Y, t) = V(L_2, Y, t) = 0, \tag{10b}$$

$$\frac{\partial \theta}{\partial X}(L_2, Y, t) = 0. \quad (10c)$$

In order to solve the above system of equations, the well-established SIMPLER numerical solution technique of Patankar [17] was employed. Typically, 30–1500 iterations were required for the local variables to achieve convergence. The convergence criterion adopted was that relative variations in velocity, temperature, and transverse temperature gradients between two successive iterations were smaller than a pre-assigned value of 10^{-4}. The well-known steady non-pulsating flow solution at the same Darcy number was used as the initial-state conditions to obtain quasi-steady periodic state results. In most cases, temporally periodic solutions were secured after 2–8 cycles of oscillation. The time resolution was such that one pulsating period was divided into 120 time steps. The spatial grid was typically 120×25 in the X–Y computational domain, which consisted of the half-width channel. The sensitivity of calculated results to the grid interval, time step, and convergence criterion was checked in several sample calculations. The computational parameters that were selected for the present work were found to yield satisfactory results in the grid- and time step-convergence tests.

3. NUMERICAL RESULTS AND DISCUSSION

In order to simulate a long channel, the geometry was selected such that $L_1 = 100.0$, $L_2 = 140.0$ (see Kim *et al.* [18]). Several exemplary calculations established that these parameter values were found to produce fully-developed flow conditions in the isothermal-wall portion of the channel. It was also shown that the imposed exit boundary conditions, equations (10a)–(10c), were compatible to a fair degree of accuracy. In an effort to perform explicit comparisons with the previous studies [11], it was set that $Re = 50.0$ and $Pr = 0.7$ in the present study. This relatively low value of Re was chosen to simulate a reasonably slow slug flow [3].

In summary, the objective here was to acquire an improved understanding of the changes in convective heat transport brought about by the introduction of flow pulsation and by the existence of the porous media. For this purpose, the problem setup was designed for a simple geometry, with the adoption of straightforward boundary conditions. The parameter values for actual computations were selected based on well-documented preceding related studies [3, 9, 11].

As emphasized earlier, the main mission of the present study is to disclose the effect of pulsation. To this end, broad ranges of the pulsation frequency ($0 \leqslant M \leqslant 10.0$) and of the pulsation amplitude ($0.15 \leqslant A \leqslant 0.75$) were considered. Of special interest are the cases when the pulsation amplitude A is appreciable. The impact of the porous media is represented by the Darcy number Da, which encompassed a wide range $10^{-4} \leqslant Da \leqslant \infty$. Furthermore, the thermal conductivity ratio R_k and the heat capacity ratio R_c were varied over ranges of $0.1 \leqslant R_k \leqslant 10.0$ and of $0.1 \leqslant R_c \leqslant 10.0$, respectively.

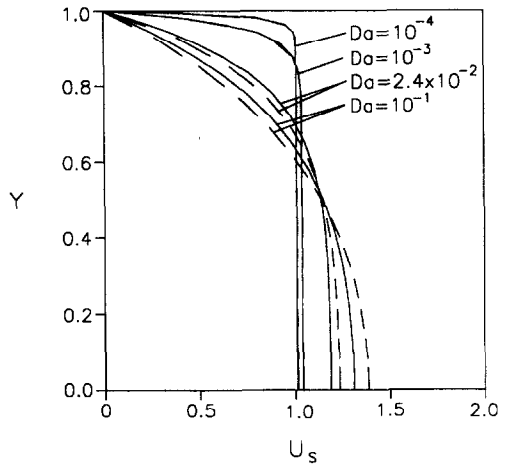

FIG. 2. Velocity profiles U_s for non-pulsating flow ($A = 0$) in the fully-developed region: (——) present calculations; (– – –) analytical solutions of Kaviany (1985).

In the first, major features of flow will be delineated in Figs. 2–6. Figure 2 illustrates the effect of Da on the fully-developed mainstream velocity profile U_s for the case of a non-pulsating inlet flow ($A = 0$). When Da is large, the profile bears resemblance to the familiar parabolic shape of the conventional Poiseuille flow in a channel with no porous medium. The influence of the porous media is characterized by the smallness of Da. As displayed in Fig. 2, as Da decreases, the overall velocity profile tends to be flat in the bulk of channel interior, and a region of steep velocity gradients is seen near the wall. The plots shown in Fig. 2 are in close agreement with the analytical predictions of Kaviany [9]. The small discrepancies for large Da are attributable to the neglect of the inertia terms in the analysis by Kaviany [9].

Scrutiny is made of the structure of the purely time-dependent part of the velocity, U_{t-s}, which is defined as $(U_t - U_s)/(B_1/B_m)$, where U_t is the total instantaneous velocity, U_s denotes the non-pulsating steady part, and B_1 and B_m the primary oscillating component and the time mean value of the axial pressure gradient, respectively. Figure 3 [$Da = 2.4 \times 10^{-2}$, $C = 0$] exemplifies the results for extremely large values of Da. This value is used to enable an explicit comparison with the essentially one-dimensional analysis of Khodadadi [11]. When the pulsation frequency parameter is low (see Fig. 3a), the velocity profiles are akin to quasi-steady-state solutions. This implies that, at each time instant, the overall velocity field is similar to that of a non-pulsating flow driven by the instantaneous pressure gradient imposed along the channel length. In the opposite limit, when M is large (see Fig. 3b), the magnitude of U_{t-s} is very small (note the difference in the scales of abscissa used in

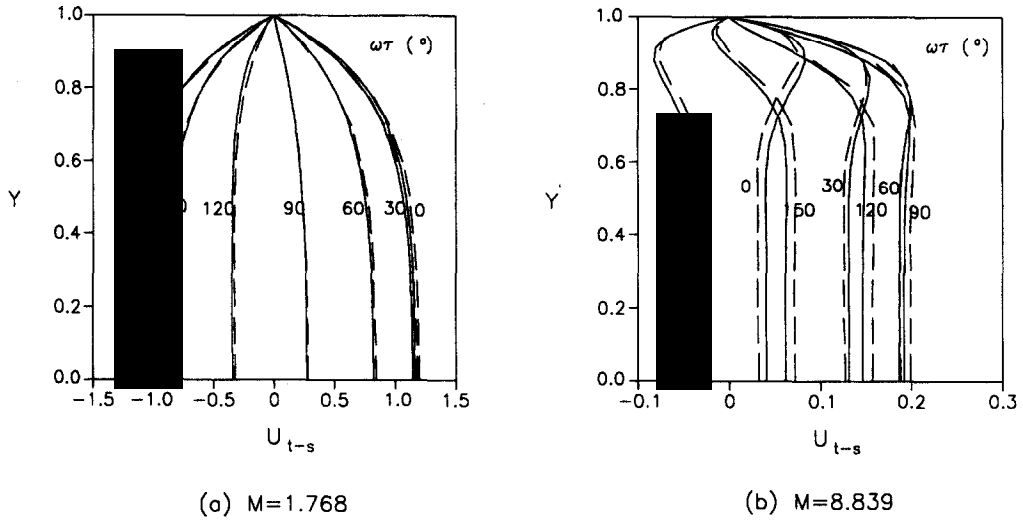

FIG. 3. Profiles of purely time-dependent part of velocity U_{t-s}: $Da = 2.4 \times 10^{-2}$; (——) present calculation; (– – –) analytical solutions of Khodadadi (1991). (a) $M = 1.768$; (b) $M = 8.839$.

Fig. 3a and 3b). Furthermore, the profiles are fairly flat in much of the channel interior, and rapid Y-variations are notable near the channel walls. These gross characteristics are qualitatively similar to the behavior of a pulsating flow in a channel with no porous media [3, 16]. Also, the present numerical results are in broad agreement with the predictions of Khodadadi [11].

The results for small Da are typified in Fig. 4. The entire channel is filled with a porous material of low permeability, and this leads to increased bulk damping for the fluid flow. In much of the whole domain inside the channel, the U_{s-t} profile is flat. Only in a narrow strip very near the wall, large velocity gradients are seen. This qualitative pattern of velocity profile is insensitive to the changes in pulsation frequency M.

The temporal variations of the axial pressure gradient B and of skin friction coefficient C_f in the fully-developed region are plotted in Figs. 5 and 6. For large Da, Fig. 5 demonstrates that, when M is small, both B and C_f are nearly in phase with the inlet velocity. However, when M is large, the phase leads of B and C_f approach approximately $\pi/2$ and $\pi/4$, respectively, and the magnitudes of the oscillating components are increased. These findings serve to reconfirm the qualitative correctness of the previous analytical results for a non-porous channel [3].

Figure 6 shows typical results for small Da. Both the phase leads and the amplitudes of oscillation of B and C_f remain virtually unaffected by the changes in M. The channel interior is filled with a porous material of low permeability, and the changes in pulsation frequency cause little qualitative alterations in the temporal behavior of B and C_f. These observations are in accord with the analytical findings of Khodadadi [11].

Processing the numerical results of the temperature

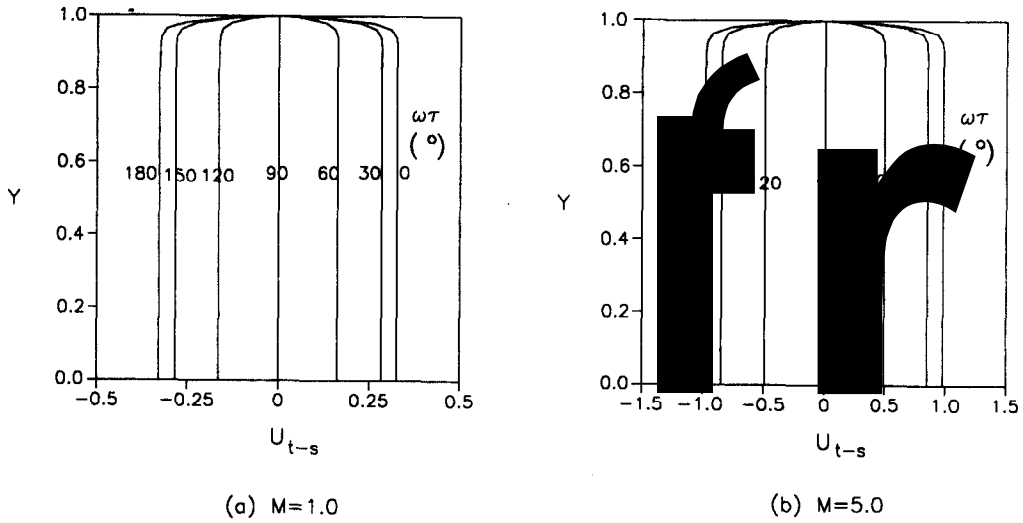

FIG. 4. Same as in Fig. 3: $Da = 10^{-4}$. (a) $M = 1.0$; (b) $M = 5.0$.

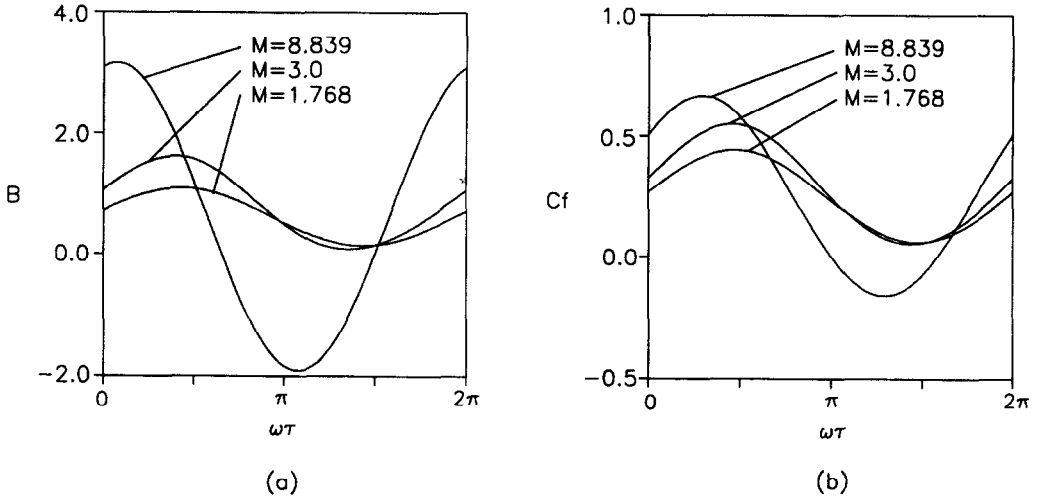

FIG. 5. Temporal variations over a cycle of: (a) axial pressure gradient, B; and (b) skin friction coefficient, C_f: $Da = 2.4 \times 10^{-2}$, $A = 0.75$.

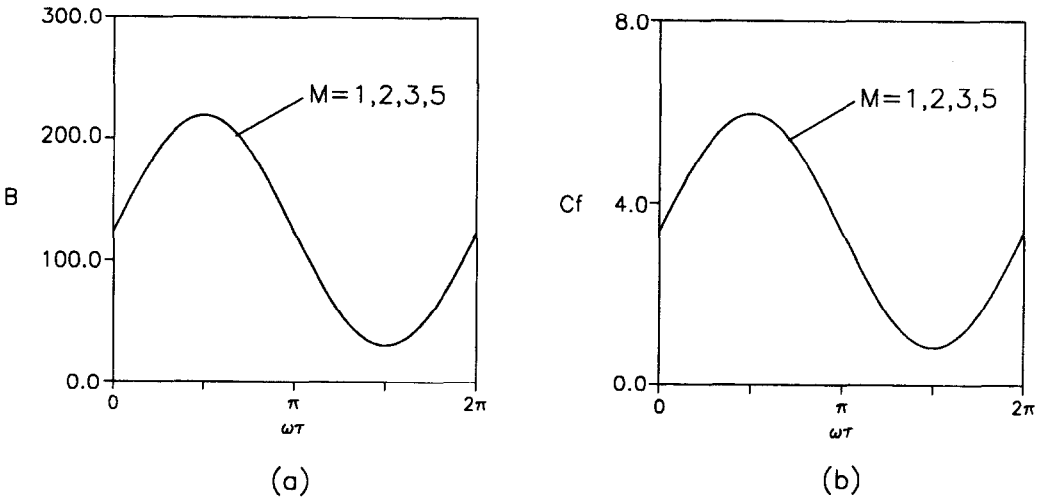

FIG. 6. Same as in Fig. 5: $Da = 10^{-4}$; $A = 0.75$.

field, the heat transfer properties are now examined. One physical quantity of interest is Nu_b, which denotes the Nusselt number based on the bulk temperature, $Nu_b \equiv 4(\mathrm{d}\theta/\mathrm{d}Y|_{Y=1})/(1-\theta_b)$. It should be stressed that heat transfer in the present context refers to the one between the channel wall and the fluid. In some studies on pulsating flows, discussions of heat transfer augmentation and/or reduction are concerned with the fluids in the upstream and the downstream locations. Before proceeding further, it is worth pointing out to what kind of heat transport the present account is directed. Figure 7 illustrates the behavior of Nu_b, for the case of a non-pulsating flow in the fully-developed region. In line with the predictions by Kaviany [9], the Darcy number is on the abscissa. As displayed in Fig. 7, the present numerical results are in good agreement with the analysis of Kaviany [9]. As expected, in the limit of a non-porous channel ($Da \gg 1$), Nu_b reaches the value of 7.54. In the other

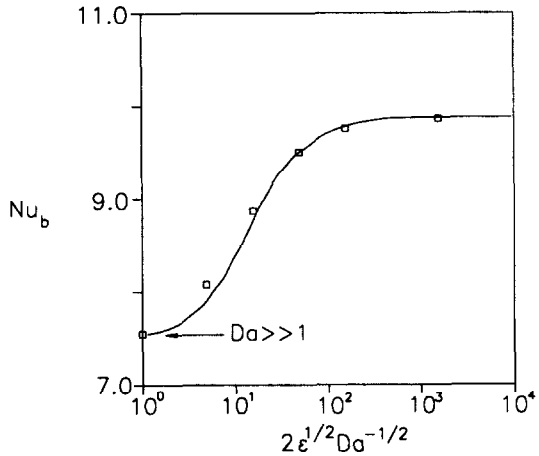

FIG. 7. Effect of Da on Nu_b in the fully developed regions for non-pulsating flow ($A = 0$), $R_k = 1.0$; □—present calculations for selected Darcy numbers; (——) analytical prediction of Kaviany (1985).

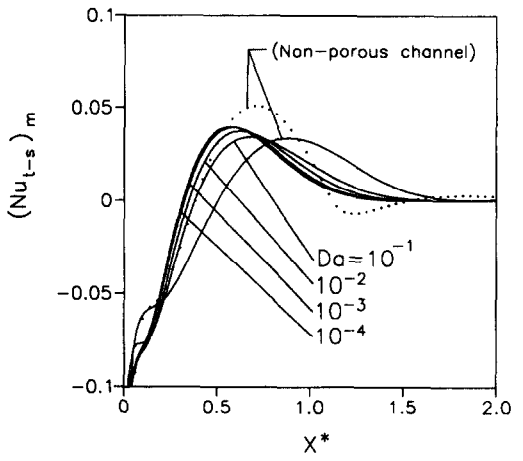

FIG. 8. Axial profiles of cycle-averaged values of time-dependent part of heat transfer, $[Nu_{t-s}]_m$: $M = 2.0$, $A = 0.75$, $R_k = 1.0$, and $R_c = 1.0$; (——) present calculations; (· · · ·) analytical solution of Siegel and Perlmutter (1962) for non-porous channel.

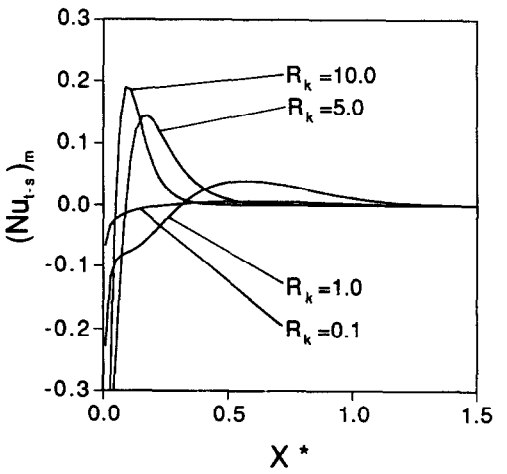

FIG. 9. Axial profiles of $[Nu_{t-s}]_m$: $M = 2.0$, $A = 0.75$, $Da = 10^{-4}$, and $R_c = 1.0$.

extreme, as Da becomes very small ($Da \leqslant 10^{-6}$), the slug flow-limit of the Darcian regime is attained and Nu_b tends to the asymptotic value of 9.87.

The difference in the local Nusselt number [Nu ($\equiv hH/k$) = $(R_k/\theta_w)\cdot(d\theta/dY)|_{Y=1}$)] between a pulsating flow and the corresponding non-pulsating flow ($A = 0$) is of interest. As seen in Siegel and Perlmutter [3] and Kim *et al.* [18], the axial position is represented by using the inverse of the Graetz number, $X^* = X/(Re\,Pr)$.

The purely time-dependent part of the Nusselt number is denoted by Nu_{t-s}. It follows that the cycle-averaged value of this quantity, $(Nu_{t-s})_m$, is a measure indicating the contribution brought forth by flow pulsation.

Figure 8 depicts the spatial variation of $(Nu_{t-s})_m$. For the entire range of Da, $[Nu_{t-s}]_m$ starts rising rapidly from negative to positive values in the entrance zone of the thermally developing region. At moderate downstream locations, $[Nu_{t-s}]_m$ reaches a maximum, and, further downstream, $[Nu_{t-s}]_m$ gradually decreases. As the location moves further downstream, $[Nu_{t-s}]_m$ decreases slowly to a value close to zero, which implies that the effect of pulsation on local heat transfer diminishes. This global behavior is consistent with the analytical results of Siegel and Perlmutter [3] for the case of a non-porous channel. The overall patterns of $[Nu_{t-s}]_m$-curves are qualitatively similar, as Da encompasses a wide range. When the channel is filled with a porous material, the peak of $[Nu_{t-s}]_m$ tends to be shifted to further upstream axial positions. This tendency can be explained by the analytical findings of Vafai and Tien [6] that the thermal boundary layer thickens, as the permeability K of a porous medium, i.e. the Darcy number Da, decreases. Consequently, the thermal entry length is reduced. Distinctions between the characteristics of a porous channel and a non-porous channel may be clearly captured by comparing the present results with the corresponding data contained in the previous paper by Kim *et al.* [18].

The effect of the thermophysical properties of a porous medium is now examined. These are represented by the thermal conductivity ratio R_k and the heat capacity ratio R_c in equation (4). Figure 9 demonstrates the influence of R_k. As anticipated, as R_k increases, heat transfer between the wall and the fluid becomes vigorous; also, the peak of $[Nu_{t-s}]_m$ moves to upstream locations. Figure 10 illustrates the effect of R_c. Note that R_c appears in the time derivative term of the temperature equation (4). Therefore, the steady-state solution is unaffected by R_c. As displayed in Fig. 10, the impact of R_c on heat transfer rates is substantial. As R_c increases, the peak of $[Nu_{t-s}]_m$ is seen to be shifted to upstream locations. It should be pointed out that, in equation (4), an increase in the value of R_c causes amplification of the time derivative term. This effect is qualitatively similar to an increase in pulsation frequency. Consequently, the overall

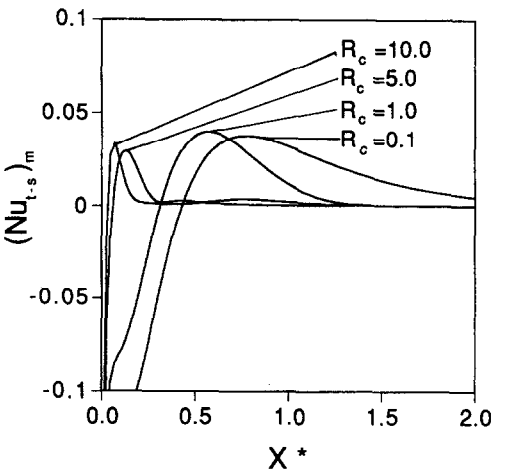

FIG. 10. Axial profiles of $[Nu_{t-s}]_m$: $M = 2.0$, $A = 0.75$, $Da = 10^{-4}$, and $R_k = 1.0$.

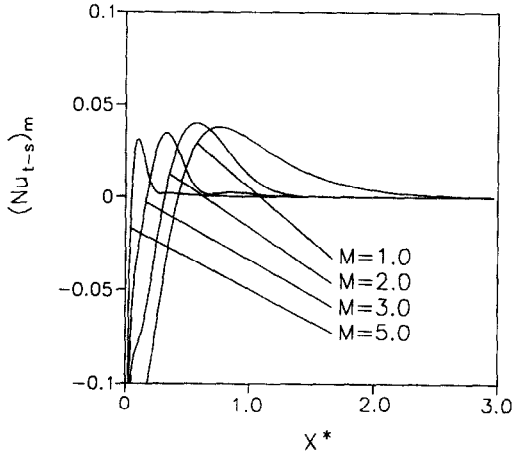

FIG. 11. Axial profiles of $[Nu_{t-s}]_m$: $A = 0.75$, $Da = 10^{-4}$, $R_k = 1.0$, and $R_c = 1.0$.

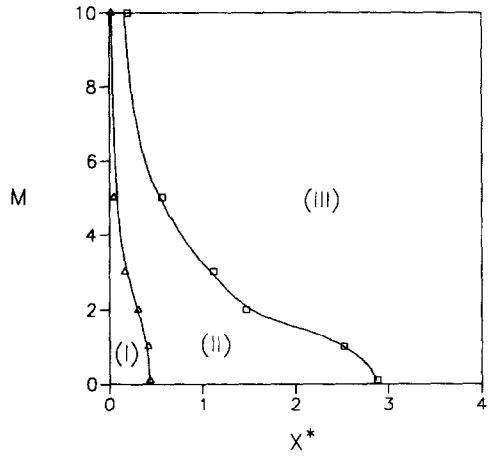

FIG. 13. Regime diagram for $[Nu_{t-s}]_m$ in the M–X^* plane: $Da = 10^{-4}$, $R_k = 1.0$, and $R_c = 1.0$

influence of R_c is akin to the role played by M, and this is verified in Figs. 10 and 11. As displayed in Fig. 11, as the pulsation frequency M increases, the peak of $[Nu_{t-s}]_m$ occurs at further upstream locations. It is notable that, when M is low, the flow pulsation leads to a substantial increase in heat transfer along much of the axial length of the channel. When M is high, heat transfer enhancement in less effective and is confined to the entrance zone of the heated channel wall. The impact of a high-frequency pulsation on heat transfer is meager in the bulk of the downstream location, and this overall behavior is similar to that caused by R_c.

The effect of the pulsation amplitude A is shown in Fig. 12. As expected, the general augmentation of heat transfer is significant as A increases.

By compiling the comprehensive numerical results, the qualitative pattern of augmentation of heat transfer may now be classified into three regimes. The regime diagram, as exemplified in Fig. 13, is constructed on the M–X^* plane (see Kim *et al.* [18]). $[Nu_{t-s}]_m$ is negative in zone (I); this implies that, at low pulsation frequencies and in the extreme upstream entrance region, the presence of pulsation reduces the heat transfer. In zone (II), $[Nu_{t-s}]_m$ is positive, which indicates an enhancement of heat transfer due to the existence of pulsation. This takes place at moderate and downstream locations; and, as M becomes large, this zone of heat transfer augmentation shrinks in size and tends to be found closer to the entrance region. At farther downstream in zone (III), the net changes of Nu due to pulsation are very small and thus of less interest (e.g. $|[Nu_{t-s}]_m| \leqslant 10^{-3}$).

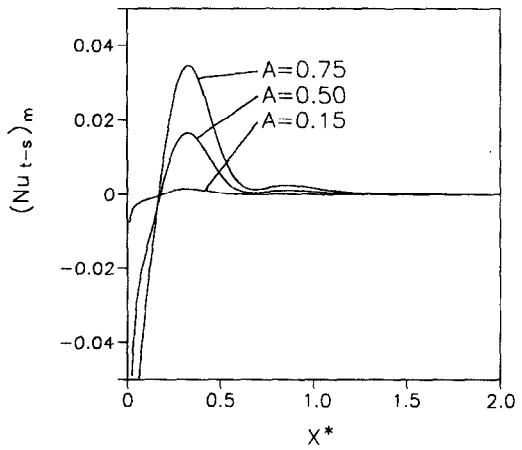

FIG. 12. Axial profiles of $[Nu_{t-s}]_m$: $M = 3.0$, $Da = 10^{-4}$, $R_k = 1.0$, and $R_c = 1.0$.

Perusal of the computed data points to the observation that the shape of the demarcation line, which divides zone (I) and (II), is determined principally by Da and M, and less by A. As Da increases, the bands of zones (I) and (II) move further downstream of the channel, and the magnitude of $[Nu_{t-s}]_m$ is reduced (see Fig. 8). The pulsation amplitude A has a strong influence on the quantitative value of $[Nu_{t-s}]_m$ (see Fig. 12); however, the gross characteristic patterns of $[Nu_{t-s}]_m$ on the M–X^* plane are little affected by A. The physical mechanism underlying the above behavior of $[Nu_{t-s}]_m$ was discussed in Kim *et al.* [18] for a non-porous channel. Basically, the non-linear interactions due to the oscillating components gives rise to a substantial increase in effective diffusivity of the flow process. Consequently, heat transfer between the isothermal channel wall and the interior fluid depends crucially on the axial gradient of the fluid bulk temperature. In comparison to the case of a non-pulsating flow, the lateral temperature gradient of a pulsation flow at the wall is reduced in the entrance region and steepened at moderate downstream locations. In the present context, this general qualitative picture prevails; however, the existence of a porous material modifies the heat transport properties in a quantitative way (see Figs. 8–10). Summing up, these numerical results should be complementary to any future experimental verifications of pulsating-flow heat transfer characteristics.

4. CONCLUSION

The computed velocity fields are in broad agreement with the prior analytical findings. When Da is large, the velocity profiles at low M are akin to the quasi-steady flows in a non-porous channel; and, for high M, only a narrow portion very close to the wall is affected. When Da is small, the effect of porous media is significant; the velocity profiles are flat in much of the channel interior. The axial pressure gradient and skin friction coefficient are little affected by the changes in M.

The effect of pulsation on heat transfer is pronounced in the upstream entrance area, typically $X/(Re\,Pr) \leqslant 1.0$. Changes in heat transfer rate due to pulsation $[Nu_{t-s}]_m$ are appreciable throughout much of the channel length when the pulsating frequency is low to moderate. At high pulsating frequencies, $M > 1.0$, abrupt changes in Nusselt number Nu are generally observed in a narrow region near the entrance region. In comparison to the case of a non-pulsating flow, $[Nu_{t-s}]_m$ is negative at low pulsation frequencies and in the extreme upstream region, and $[Nu_{t-s}]_m$ is positive at moderate downstream locations. At locations further downstream, $[Nu_{t-s}]_m$ is virtually zero. As Da decreases or R_k increases, the peak value of $[Nu_{t-s}]_m$ increases; also, the location of the peak value of $[Nu_{t-s}]_m$ moves upstream. The peak value of $[Nu_{t-s}]_m$ tends to be shifted to further upstream locations as R_c increases.

Acknowledgements—Appreciation is extended to the referee who provided constructive and useful suggestions. This work was supported in part by research grants from MOST and KIST of Korea.

REFERENCES

1. S. Uchida, The pulsating viscous flow superposed on the steady laminar motion of incompressible fluid in a circular pipe, *ZAMP* **VII**, 403–422 (1956).
2. M. J. Lighthill, The response of laminar skin friction and heat transfer to fluctuations in the stream velocity, *Proc. Roy. Soc.* **224**, 1–23 (1954).
3. R. Siegel and M. Perlmutter, Heat transfer for pulsating laminar duct flow, *Trans. ASME J. Heat Transfer* **84**, 111–123 (1962).
4. U. H. Kurzweg, Enhanced heat conduction in oscillating viscous flows within parallel-plate channels, *J. Fluid Mech.* **156**, 291–300 (1985).
5. T. W. Simon and J. R. Seume, A survey of oscillating flow in Stirling engine heat exchangers, NASA Contractor Report 182108 (1988).
6. K. Vafai and C. L. Tien, Boundary and inertia effects on flow and heat transfer in porous media, *Int. J. Heat Mass Transfer* **24**, 195–203 (1981).
7. D. Poulikakos and A. Bejan, The departure from Darcy flow in natural convection in a vertical porous layer, *Physics Fluids* **28**, 3477–3484 (1985).
8. G. Lauriat and V. Prasad, Non-Darcian effects on natural convection in a vertical porous enclosure, *Int. J. Heat Mass Transfer* **32**, 2135–2147 (1989).
9. M. Kaviany, Laminar flow through a porous channel bounded by isothermal plates, *Int. J. Heat Mass Transfer* **28**, 851–858 (1985).
10. D. Poulikakos and K. Renken, Forced convection in a channel filled with porous medium, including the effects of flow inertia, variable porosity, and Brinkman friction, *Trans. ASME J. Heat Transfer* **109**, 880–888 (1987).
11. J. M. Khodadadi, Oscillatory fluid flow through a porous medium channel bounded by two impermeable parallel plates, *Trans. ASME J. Fluids Engng* **113**, 509–511 (1991).
12. N. Kladias and V. Prasad, Flow transitions in buoyancy-induced non-Darcy convection in a porous medium heated from below, *Trans. ASME J. Heat Transfer* **112**, 675–684 (1990).
13. K. Vafai and C. L. Tien, Boundary and inertia effects on convective mass transfer in porous media, *Int. J. Heat Mass Transfer* **25**, 1183–1190 (1982).
14. M. Kaviany, *Principles of Heat Transfer in Porous Media*. Springer-Verlag, New York (1991).
15. T. S. Ludgren, Slow flow through stationary random beds and suspensions of spheres, *J. Fluid Mech.* **51**, 273–299 (1972).
16. E. B. Denison, W. H. Stevenson and R. W. Fox, Pulsating laminar flow measurements with a directionally sensitive laser velocimeter, *A.I.Ch.E. Jl* **17**, 781–787 (1971).
17. S. V. Patankar, *Numerical Heat Transfer and Fluid Flow*. Hemisphere, New York (1980).
18. S. Y. Kim, B. H. Kang and J. M. Hyun, Heat transfer in the thermally developing region of a pulsating channel flow, *Int. J. Heat Mass Transfer* **36**, 4257–4266 (1993).